Strong room-temperature blue emission from rapid-thermal annealed cerium-doped aluminum (oxy)nitride thin films

Alaa E Giba, Philippe Pigeat, Stéphanie Bruyere, Hervé Rinnert, Flavio Soldera, Franck Mücklich, Raul Gago, David Horwat

Strong room-temperature blue emission from rapid-thermal annealed cerium-doped aluminum (oxy)nitride thin films

A.E. Giba[1,2,3], P. Pigeat[1], S. Bruyere[1], H. Rinnert[1], F. Soldera[2], F. Mücklich[2], R.Gago[4], D. Horwat[1*]

[1]*Institut Jean Lamour – UMR CNRS 7198– Université de Lorraine, Nancy, France.*

[2]*Department Materials Science and Engineering, Saarland University, D-66123 Saarbrücken, Germany.*

[3]*National Institute of Laser Enhanced Sciences, Cairo University, Giza 12613, Egypt*

[4]*Instituto de Ciencia de Materiales de Madrid, Consejo Superior de Investigaciones Científicas, E-28049 Madrid, Spain.*

* contact :david.horwat@univ-lorraine.fr

Abstract

Cerium-doped aluminum nitride (Ce-AlN) thin films were prepared at room temperature (RT) using radio frequency (RF) reactive sputtering. As-grown samples were then subjected to rapid thermal annealing (RTA). X-ray diffraction and high resolution transmission electron microscopy (HRTEM) revealed a well crystalline textured microstructure with single [002] out-of-plane orientation in both as-grown and annealed samples. A strong RT blue emission from post-deposition annealed samples was detected when excited by 266 and 325 nm laser. Electron energy loss spectroscopy (EELS) at the Ce edges reveal the dominant oxidation state of Ce atoms, which undergoes a change from of Ce^{4+} to Ce^{3+} ions after RTA annealing in Ar atmosphere. The chemical composition was analyzed by Rutherford backscattering spectrometry (RBS) and contrasted to HRTEM images. Our findings indicate that the surface oxidation during the post-deposition annealing in Ar plays an important role in the PL response by changing the oxidation state of Ce ions from optically inactive ions (Ce^{4+}) to the optically active ones (Ce^{3+}). Moreover, the importance of this oxidation is further confirmed by the excitation mechanisms responsible for blue emission determined by PL excitation measurements.

Keywords : AlN; Ce; photoluminescence, oxidation state, EELS

Optical blue emission attracts great attention since it is an important component for generating white light emitting devices (LEDs). Among them, white light-based LEDs (w-LEDs) exhibit many advantages over the conventional lamps such as longer lifetime, higher quantum efficiency, lower energy consumption and environmental friendliness.[1] These facts make w-LEDs cost-efficient optical sources to replace the traditional light sources. In addition, w-LEDs are highly desirable from technological point of view through their applications in smart-phones, computer screens, TVs, etc. It is known that bright white light can be obtained from the combination of the three RBG colors.[2] Thus, two common methods have been developed to create w-LEDs. First, the multi-LED chips that contain three individual LEDs with blue, green and red colors which mixing results in white light. The second is the phosphor conversion LED that contains blue or ultraviolet (UV) emitters with yellow or multicolor phosphors. In both methods, blue emission is needed. Although green and red LEDs have been obtained since the 1950s,[3] achieving blue LEDs was challenging since it requires more energetic photons emitted from special materials with wide/direct bandgap and high crystal quality. The first blue LEDs made from high quality indium-doped gallium nitride was produced in the early 1990s.[3] Intense research activities are still devoted to the generation of blue light emission by searching for new phosphors. One of the most common ways to activate the blue emission is doping a wide bandgap semiconductor by rare earth (RE) elements. In this line, Ce^{3+} and Eu^{2+} are the most frequently used activators due to their luminescence properties attributed to fully allowed electric dipole 5*d*-4*f* transitions that lead to a large absorption cross section in UV-visible range.[4-8] However, Ce^{3+} is particularly interesting due to its fast and efficient luminescence in UV-blue regions.[9-10] Ce^{3+} has only one electron in its 4*f* state. Hence, the excited 5*d* level becomes unshielded from the crystal field effect, resulting in spectral properties strongly affected by the surrounding environment (crystal field strength, symmetry, covalence/ionic characters).[9, 11] Since its luminescence properties can be controlled and enhanced by the local environment of Ce ions, the search for appropriate host materials is a priority. Beside the common

requirements for a good host material (high crystallinity, reliability and high transparency, etc.), the chemical and thermal stability of the phosphors is highly desired for better device performance at high temperature operation. Moreover, the strong absorption of the UV and blue light is required for high quantum conversion efficiency in blue or UV LEDs. Among reported possible host systems for RE doping, (oxy)nitride-based materials offer high thermal/chemical stability, good luminescence properties and tunable excitation/emission spectra by controlling the ratio between the nitrogen and oxygen content.[1] The above excellent characteristics of the nitrogen based compounds were referred to the contribution of nitrogen atoms in the bonding system of the material.[12] Thanks to the lower electronegativity of nitrogen atoms compared to oxygen ones, the covalent character of (oxy)nitride compounds is higher than that of the pure oxide counterpart. This makes, in turn, the crystal network structure more rigid and enhances both the thermal and chemical stability.[12] Moreover, due to the higher formal charge of N^{3-} than O^{2-}, a stronger crystal field splitting is induced and affects the surrounding cations, shifting the lowest *d* orbital of Ce to lower energy.[13-14] Hence, the excitation and emission of Ce ions can be tuned by modifying the N/O ratio. Among the nitride family, we focus in this work on aluminum (oxy)nitride materials for the following reasons. First, aluminum nitride (AlN) has a direct and wide optical bandgap (6 eV) with high transparency in UV-visible range that can offer the opportunity to cover wide range of colors with low thermal quenching effect.[15] Second, there are few reports dealing with Ce-doped AlN. For example, amorphous Ce-AlN thin films were prepared by DC magnetron co-sputtering on heated substrates up to 350ºC.[16] Their structure and microstructure was studied but the assignment of the photoluminescence (PL) signal was not clear. Liu *et al.*,[17] studied in more detail the blue emission from a polycrystalline powder of AlN phosphor co-activated by Ce^{3+} and Si^{4+} synthesized by gas pressure sintering under high temperature (2050ºC for 4 hr) and high nitrogen pressure (0.92 MPa). Also, an intense luminescence at 600 nm from Ce-doped single-crystal AlN bulk synthesized by reactive flux method under high pressure/temperature was also reported.[18-19] The authors succeeded to directly observe the diffusion of single Ce atoms.[19] Recently, A. Majid *et al.*,[20-21] demonstrated theoretically the modification of the electronic structure of Ce-doped AlN using first principle calculations. More recently,

broad-band emission from Ce-doped AlN ceramic bulk material sintered at (1700ºC and 105 MPa) has been reported,[22] but experimental evidence of the influence of Ce oxidation state on the optical emission is still missing. Hence, deep investigation of Ce-doped AlN thin films, compatible with the chip technology, is particularly desired.

Based on the above, this work is dedicated to the synthesis and study of the optical properties of crystalline Ce-doped AlN thin films grown at room temperature (RT) by radiofrequency (RF) magnetron sputtering. Strong blue emission has been obtained from the activated Ce ions after rapid thermal annealing (RTA) in Ar atmosphere. The origin of the blue emission is investigated by Electron Energy Loss Spectroscopy (EELS), PL and PL excitation (PLE) experiments. To the best of knowledge, this is the first work reporting on the synthesis of crystalline Ce-doped AlN thin films on silicon substrates by this method.

Experimental section

Undoped and Ce-doped AlN thin films were deposited using RF (Dressler, CESAR RF power generator) balanced reactive magnetron sputtering at RT. A high vacuum pressure of 10^{-6} Pa was obtained by using a turbo molecular pump (BOC EDWARDS EXT 255HI) coupled to a mechanical primary pump. An aluminum disk (99.99% purity, neyco vacuum & materials) of 2 inch diameter was used as sputtering target for the AlN film preparation. For Ce-doped AlN films, a modified Al target was used that incorporates a thin bar of metallic Ce (99.9% purity, neyco vacuum & materials) with appropriate relative surface area Ce/Al about 0.027 in order to obtain ~1% of Ce in the deposited films. Silicon (100) substrates have been ultrasonically cleaned in ethanol and fixed at 5 cm distance from the Al target, facing the target axis. The deposition time was adjusted for each deposition condition to reach a thickness close to 200 nm as monitored *in-situ* by laser interferential reflectometry. The films have been deposited under gas composition of 65% N_2, working pressure 0.6 mtorr and RF power 100 W. Al-rich and N-rich samples have been deposited under the same experimental conditions as for Ce-doped sample except the gas composition was set to 30% N_2 and 100% N_2 for Al-rich and N-rich, respectively. The as-grown samples were divided into different pieces that underwent

post-deposition RTA treatments at 1000ºC in Ar (Air liquide, ALPHAGAZ 2 ARGON) and forming gas (FG) N_2/H_2 (Air liquide GSF, N_2/H_2 %=90/10) for 5 minutes.

The crystal structure and growth orientation of the films were analyzed by X-ray diffraction (XRD) in a Brucker D8 Advance system with Cu $K_{\alpha 1}$ radiation (λ= 0.15406 nm) in Bragg-Brentano geometry. The samples were shined only with Cu $K_{\alpha 1}$ radiation. A LINXEYE XE linear detector was used that exhibits excellent filtering of K_β radiation without the need of secondary monochromator. All samples were positioned on substrate holders and aligned with a reference plane of the holders. Holders were enabled to spin around their vertical axis during measurement with integration time of 1 hour. The full width at half maximum (FWHM) of the (002) peak has been estimated after subtracting the instrumental broadening of 0.09°. Details of the microstructure were investigated by transmission electron microscopy (TEM) in a JEOL ARM 200-Cold equipped with a field-emission gun (FEG) fitted with a GIF Quantum ER. Electron Energy Loss Spectroscopy (EELS) coupled to the TEM instrument has been used for investigating the oxidation states of Ce ions. For the acquisition of EELS spectra, an accelerating voltage of 200 kV, an emission current of 15 μA and an energy dispersion of 0.05 eV/ch were employed. All EELS spectra were recorded in image mode, with an energy resolution of 0.55eV defined by the full width at half maximum (FWHM) of the zero loss peak. Compositional analysis was performed by Rutherford backscattering spectrometry (RBS) with a 2 MeV He^+ beam. The experiments were performed with the 5MV accelerator available at *Centro de Microanálisis de Materiales* (CMAM) from Universidad Autónoma de Madrid (Madrid, Spain).

Finally, the steady state PL experiments were performed at RT. Samples were excited either by the 325 nm line of an He–Cd laser or by a frequency-quadruped YAG:Nd^{3+} laser emitting at 266 nm. For PLE spectroscopy, the samples were excited by a xenon arc lamp source. PL emission was analyzed by a cooled silicon-based CCD camera.

Results and discussion

X-ray diffraction (XRD)

Fig (1) shows the XRD measurements of as-grown (As) and RTA samples in Ar or FG atmospheres. All spectra reveal the characteristic peak of (002) plane of the hexagonal wurtzite type structure of AlN, with the basal planes parallel to the substrate surface. No traces of metallic cerium could be detected within detection limits in the X-ray diffractograms with 2θ angles ranging from 20° to 120° (see the supporting information figure S1). Moreover, metallic cerium was not detected using high resolution TEM at different positions throughout the films. The shift of the AlN reflection suggests that Ce atoms were incorporated in the AlN crystal lattice. In particular, the diffraction peaks of doped samples shifted to lower diffraction angles, indicating the incorporation of Ce expands the c-axis parameter, likely due to in-plane compressive stress induced by the large volume of Ce ions.[23] The average c-axis parameters of the prepared samples has been estimated using Bragg's law[24] and is found to be increased from 4.97 A^0 to 5.04 Å for undoped and doped samples, respectively. However, the XRD of the doped samples didn't show any reflection from other planes than (002) related to AlN within the detection limit. This indicates that, although the doping with 1% of Ce, the films exhibit crystallites with c-axis orientation normal to the substrate surface like undoped films.[25] The undoped sample annealed in Ar exhibits higher (002) intensity than the as-deposited one. In contrast, doped samples present lower diffraction intensity with respect to the undoped counterpart and, in addition, a further intensity decrease after annealing. This could be attributed to the influence of thermal treatment that can enhance the crystallinity of undoped AlN by curing the material defects[26] whereas in doped AlN the presence of the foreign atoms (Ce) inside the lattice could generate more defects under the thermal treatment by initiating new kind of bonds with the surrounding atoms that degrade the crystal lattice structure. The degradation of XRD intensity in the doped samples in comparison to the undoped counterpart is a familiar effect, particularly when the dopant atoms have larger ionic size than the native atoms. The degradation of the crystallinity is usually attributed to the lattice stress induced by the foreign atoms. In most cases the dopant atoms have either size and/or valance state mismatch with the substituted atoms that disturb the local environment. In our case, the ionic radii of cerium ions Ce^{4+} (101 pm) and Ce^{3+} (115 pm) are much larger than the ionic radius of Al^{3+} (67.5 pm). Effective substitution of Al by Ce leads to local changes in the crystal lattice and, in turn, affects

the electronic structure of the material.[27] The change in the XRD linewidth and the increase of c-axis parameter are indicative parameters of the microstructure modifications. For instance, the average strain over whole the thickness of the film (macrostrain) results in change in the c-axis and, in turn, shifting of the XRD signals. A significant shift in the XRD (002) peak position towards lower values in the diffraction angles is observed in the doped samples with respect to undoped ones, see table I. This indicates that incorporation of Ce ions introduces strong macrostrain. The phase vapor condensation process itself can lead to macrostrain in undoped coatings with respect to the c-axis parameter for bulk AlN. The macrostrain along the c-axis is calculated for all samples using the following expression :

$$(c-c_0)/c_0, \quad (1)$$

where c_0= 4.978 Å is the *c*-axis value of the unstrained sample and c is calculated from the position of the (002) reflection.[28] On the other hand, the FWHM broadening of XRD is associated to the local structure (microstrain) induced by structure disorders, boundaries and dislocations as well as the small size of crystallites.[28-29] Hence, the FWHM broadening is considered as a combination of the small crystal size and the microstrain. In this regard, Williamson-Hall (WH) method can be used to determine the microstrain by considering two integral line breadth components at 002 and 004 diffraction angles, (see the supporting information figure S 2). The microstrain values for undoped AlN films, table I, exhibit a local strain relaxation after annealing the film, while doping with Ce ions induces a significant microstrain. The microstrain values for annealed Ce-AlN samples couldn't be determined because the (004) intensity was too small to be used in the microstrain estimation even after long integration time.

table I

	AlN_As	AlN_RTA	Ce-AlN_As	Ce-AlN_FG	Ce-AlN_Ar
FWHM (002)	0.2	0.16	0.18	0.25	0.44
Peak position (°)	36.10	36.06	35.69	35.63	35.61
Macrostrain	- 0.0014	-0.0002	0.0095	0.0113	0.0119
Microstrain	0.083	0.055	0.100	----	----

Moreover, Ce-doped AlN_Ar sample is associated to weakest diffracted intensity and broadest FWHM with hump at higher angles, which infers microstructural modification occurred after annealing in Ar. On other side, doped samples after RTA in FG exhibit a less asymmetric XRD peak, indicating that annealing in Ar induces a more substantial modification of the structure. This is in line with the RBS and TEM observations in the next section.

Microstructure and composition

Fig (2) shows the TEM images and the corresponding selected area electron diffraction (SAED) for as-grown and RTA samples. All samples exhibit textured structure with columns aligned in the growth direction and c-axis of the wurtzite cell of AlN perpendicular to the substrate. The SAED of the undoped sample shows that (002) spots are more localized compared to those of doped samples which are slightly elongated. This indicates a slight misorientation of the (002) planes with respect to the film surface due to incorporation of the Ce ions. The TEM image of the doped sample after RTA in Ar evidences a bilayer structure, see fig (2 g). The top layer (about 35 nm-thick) exhibits granular crystallites with oxygen content ~20%, as determined by fitting the RBS spectrum of fig (3), while the bottom layer is columnar with less than 1% of oxygen. A similar surface modification phenomenon in post-deposition annealed films has been reported previously in RE-doped GaN.[30] It was attributed to the release of N surface atoms out of the sample during the annealing at high temperature (above 800ºC) leaving N vacancies that could cluster to form voids and change the crystal structure. In addition, at high annealing temperature the partial pressure of residual oxygen inside the oven significantly increased.[31] Hence, as (N) atoms diffuse out of the film, residual oxygen atoms find an open way to substitute the (N) sites and alter the microstructure. Fig (3) shows the RBS spectra for *as-deposited* and after RTA in Ar for a Ce-doped sample. The regions corresponding to the different elements are labelled for identification. For each film-containing element (N, O, Al, and Ce), the eventual maximum energy of backscattered projectiles is given by the kinematic factor of the collision and corresponds to scattering events occurring at the surface. This energy increases with the atomic number of the scattering center. Events (counts) at lower energy correspond to collisions

deeper in the sample since part of the projectile energy is lost in the way in and out of the sample. Hence, the broadness and shape of the film-containing elements is an indication of the film thickness and the elemental profile, respectively. Regarding the substrate signal, the thicker the film the lower the energy onset. Note that, due to the similar mass of Al and Si, the signal from both elements is partially overlapped. Also, since N and O are lighter than Si, their signal appear superimposed to that from the substrate. In the case of the as-deposited film, fitting of the RBS spectra indicates a relatively homogeneous film composition over the whole film thickness. However, as mentioned above, annealing in Ar result in a bilayer structure as evidenced from the step in the Ce signal. Here, the decrease in intensity at higher energies reflects a Ce depletion in the near surface region. In parallel, this surface layer is highly oxidized as derived from the appearance of narrow O band that corresponds to the near-surface region. This region in the annealed sample also contains a lower Al content as compared to the as-deposited one as extracted from the decreased Al intensity, see inset table fig. (3).

To evaluate the influence of the annealing atmosphere on local bonding, one can consider the following thermodynamic equilibrium equation[31]:

$$\frac{4}{3}AlN + O_2 = \frac{2}{3}Al_2O_3 + \frac{2}{3}N_2, \quad (2)$$

that works in the forward direction at high O_2 pressure (case of Ce-AlN after RTA in Ar) to stabilize Al-O bonds and in the reverse direction when the N_2 pressure increases to stabilize Al-N bonds (case of Ce-AlN after RTA in FG). Hence, the latter explains why the surface of samples annealed in FG remains smooth. In addition, the increase in oxygen content is higher than the decrease in nitrogen one. This is in line with the some reports that oxygen atoms form $Al_{0.66}O$ as they substitute nitrogen in AlN.[32-34] Therefore, one Al vacancy (V_{Al}) is generated every three O atoms.

Photoluminescence (PL) and Photoluminescence excitation (PLE)

Figure 4 (a, b) shows the RT PL with excitations at 325 nm and 266 nm. The PL shows the same behavior under both excitation wavelengths. Ce-AlN sample after RTA in Ar exhibits a strong blue PL intensity as compared to the other samples. The broad PL band

is centered at 500 nm and the blue emission can be clearly seen by the naked eye, as shown in the inset of Fig.4a. This PL band is in good agreement with a Ce-related emission. Other samples, undoped and doped (as-deposited and after RTA in FG), show one order of magnitude weaker PL intensities than the Ce-AlN sample annealed in Ar, as seen in the inset of fig (4a). These weak PL bands (400-600nm) are usually observed in AlN and attributed to defects inside the bandgap. These defects have mostly been assigned to V_{Al} and oxygen related defects.[35-37] It has been reported that post-deposition annealing of RE-doped phosphors activate the luminescence by modifying the local environment of the RE ions.[38-39] For instance, it has been demonstrated that thermal annealing (TA) of Sm-, Eu- and Yb-doped amorphous AlN thin films leads to activation of the RE ions by promoting some structural rearrangements and curing the matrix from defects.[40] In the latter work, it was proposed that the significant improvement of the PL after TA is correlated with the suppression of tail defect states and with the reduction of the probability of non-radiative pathways. Interestingly, the strong PL enhancement in our Ce-AlN sample after RTA in Ar is in good agreement with the enhancement factor reported[38] after TA under the same conditions. This suggests that AlN films doped with different REs require similar TA treatments to activate a strong PL emission. However, our results show that the PL intensity not only relies on the temperature or duration of the annealing process but also on the type of atmosphere. One can conclude that the post annealing treatment has two contributions. First, thermal assistance reduces the density of non-radiative defects by rearranging the film structure. Second, the annealing environment plays the major role, probably, because it generates and controls the type of defects inside the structure as already demonstrated for other materials.[41-43] Hence, the PL behavior could be understood by considering the activation mechanism of the Ce ions. Ce ions exist in two different stable oxidation states, Ce^{+4} and Ce^{+3}. Ce^{4+} has no electron in its outer shell orbital ($4f^{0}$). It can therefore be considered as optically inactive while Ce^{+3} has only one electron in its $4f^{1}$ state that can be responsible for optical emission by $4f$-$5d$ transitions. Thus, to better understand the PL results and gain information about Ce oxidation state, EELS measurements have been performed, see fig (5). EELS is a useful method to determine the oxidation state of Ce, characterized by two lines referred to M_5 andM_4 band edges at 883 eV and 901 eV, respectively. These features are associated to

the orbital splitting of 3*d*-4*f* transitions. Fig (5a) shows the EELS spectra for CeO_2 (Ce^{4+}) and CeF_3 (Ce^{3+}) reference samples where the presence of Ce^{4+} can be mainly distinguished by a shoulder, absent in Ce^{3+}, at 5 eV above those of the two main peaks. In addition, in some reported cases a characteristic shoulder for Ce^{3+} appears at lower energy in the M_4 peak. [44] Another method developed to evaluate the Ce oxidation state from EELS is the intensity ratio between M_4/M_5, being 0.92 for Ce^{3+} in CeF_3 and 1.3 for Ce^{+4} in CeO_2.[44] Considering all the above methods to determine the Ce oxidation state, we found that all doped samples exhibit EELS spectra corresponding to the Ce ions edges in agreement with the reported spectra elsewhere.[44-45] Fig (5b, 5c) show that the EELS of Ce-AlN films as-deposited and after RTA in FG are very close to the signature of Ce^{4+}. This means that the predominant oxidation state in these samples is optically inactive, consistently with the very weak PL. EELS measurements have also been performed at different areas in the Ce-AlN samples after RTA in Ar. EELS probed from the top layer (containing oxygen) exhibits predominance of Ce^{3+}, whereas that from the bottom layer shows predominant Ce^{4+} oxidation state as seen in fig (5d). It means that the presence of oxygen could play a major role in the activation of Ce ions by changing the valence state from +4 to +3. Moreover, we can infer that the PL of this sample mostly originates from the top layer, which raises the question about the role of oxygen in the PL behavior. As mentioned before in the microstructure section, incorporating oxygen in AlN matrix can lead to the formation of aluminum vacancies $(V_{Al})^{3-}$. $(V_{Al})^{3-}$ acts as deep acceptor level in AlN[46] and can participate in the absorption process by sharing one of its electron with either the conduction band or shallow donors.[37] Knowing that oxygen incorporated in AlN introduces a O_N^+ shallow donor level,[46] all O atoms have a neighboring V_{Al} according to Mäki *et al.*[47] Hence, $(V_{Al})^{3-}$ is likely coupled to O_N^+ to form single and/or doubly negatively charged $(V_{Al}\text{-}O_N)^{2-}$ and $(V_{Al}\text{-}2O_N)^{1-}$ complexes depending on the oxygen concentration, which is consistent with previously reported works.[37, 48] In addition the released electron from formation of O_N^+ donor levels may be responsible for the valance state change of Ce^{4+} to Ce^{3+}. Further, Ishikawa *et al.*[18] reported another energetically stable defect complex that involves Ce^{3+} where $(V_{Al})^{3-}$ connects with nearby Ce_{Al} in Ce-doped AlN material. This kind of defects may explain the predominance of

Ce^{3+} in the EELS of the top layer, indicating that the strong PL emission can be interpreted by 5*d*-4*f* transition.

To investigate the excitation mechanism for the Ce-AlN sample after RTA in Ar, PLE has been measured for the emission peak at 500 nm, as shown in fig (6). It reveals two broad excitation bands around 3.9 eV and 4.8 eV. Several experimental measurements such as cathodoluminescence and PL revealed that defect complexes $(V_{Al}\text{-}O_N)^{2-}$ and $(V_{Al}\text{-}2O_N)^{1-}$ give rise to an absorption band around 3.9 eV and 4.7 eV, respectively.[48-52] Consistently, Qimin *et al.*[36] found by hybrid-functional calculations that $(V_{Al}\text{-}O_N)^{2-}$ in AlN materials is responsible for an absorption band around 3.9 eV (317nm) due to electronic transitions $[(V_{Al}\text{-}O_N)^{2-} \Rightarrow (V_{Al}\text{-}O_N)^{1-} + e)]$. It is worth noting that the absorption peak of this transition is very close to the absorption band of Ce^{3+}.[53-55] It is also reported that another electronic transition $[(V_{Al}\text{-}2O_N)^{1-} \Rightarrow (V_{Al}\text{-}2O_N)^{0} + e]$ is responsible for an absorption band at an energy higher than 4.3 eV that depends on the oxygen content. Hence, the first band (3.9 eV) can be assigned either to the defect transition $(V_{Al}\text{-}O_N)^{2-/1-}$ [36]or to the absorption band of Ce^{3+}.[5, 56] The second band (4.8 eV) can be referred to an $(V_{Al}\text{-}2O_N)^{1-}$ complex at high oxygen concentrations, as reported elsewhere.[34, 36, 47] The excitation mechanism (either direct or indirect) for Ce^{3+} ions, when excited by 325 nm, is then rather difficult to determine due to the overlapping between the excitation bands for Ce^{3+} and $(V_{Al}\text{-}O_N)^{2-}$ complex at 3.9 eV. The high absorption cross section of Ce^{3+} stimulates the assignment of the band at 3.9 eV mainly to the direct absorption of Ce^{3+}. Nevertheless, the indirect excitation mechanism of Ce^{3+} ions via $(V_{Al}\text{-}O_N)^{2-}$ complex cannot be excluded from several aspects. First, a good agreement is found between the excitation peak around 3.9 eV in our Ce-doped AlN sample and the reported absorption peak of the complex $(V_{Al}\text{-}O_N)^{2-}$ in AlN.[36, 49, 51] Second, indirect excitation can be very efficient in several RE-doped III-V semiconductor compounds.[57-58] Third, the PLE peak at 4.8 eV demonstrates that Ce^{3+} ions can be efficiently indirectly excited. Furthermore, indirect excitation of Ce was tested by the detection of PL excited by 266 nm laser (4.66 eV) close to the 4.8 eV band and away from the absorption band suspected to belong to Ce^{3+}, see fig (4b). Then, when the sample is pumped at 325 nm, direct and indirect excitations can occur simultaneously. Direct excitation arises from the absorption by Ce^{3+} transferring an electron from 4*f* orbital to 5*d* orbital and emitting photons at 500 nm

during the relaxation process. Indirect excitation can be achieved via energy transfer from excited $(V_{Al}\text{-}O_N)^{2-}$ defect to a nearby Ce^{3+} ion.

Finally, to emphasize on the role of the defect complexes in the PL, two samples have been prepared with either Al-rich (formation of V_{Al} is energetically difficult) or N-rich conditions (formation of V_{Al} is relatively easier). These samples have then been annealed in Ar atmosphere. Fig (7) shows the PL of these samples excited by 325 nm. The PL intensity of the N-rich sample is stronger than that of Al-rich sample, which is consistent with the excitation mechanisms proposed. In other words, increased in PL is stimulated by higher density of V_{Al} that leads to more activated Ce^{3+} ions and/or higher density of $V_{Al}\text{-}O_N$. This confirms the significant role of V_{Al}-related defects in the PL and supports the previous explanations.

Conclusion

This work mainly focused on understanding the PL response of Ce-doped AlN thin films prepared by a low-cost and industrial oriented technique such as RF reactive magnetron sputtering. Optical activation of the Ce dopants was achieved by RTA of as-grown samples. It was found that the incorporation of oxygen in the film was essential to promote the PL response in the samples. In addition, Al vacancies and related defect complexes have a significant role on the excitation mechanisms of Ce^{3+}, hence increasing the PL intensity. This role was confirmed by the PL measurements of Al-rich and N-rich samples. Indirect excitation of Ce ions was proposed from PLE experiments showing excitation of the blue emission related to Ce^{3+} by defect complexes. The strong blue emission in this new (oxy)nitride-based materials holds great potential for solid state lighting applications due to its thermal and chemical stability as well as the luminescence efficiency. The comprehensive approach conducted within this study could serve as a guideline for better understanding and engineering the luminescence in RE-doped (oxy)nitride thin films.

Acknowledgements

A.E. Giba thanks Erasmus mundus scholarship that financially funded this work within the DocMASE program. He also thanks the Université franco-allemande (UFA) for

supporting his travel and stay to Saarland University within the PhD track in Materials Science and Engineering. Financial support from grant P2013/MIT-2775 (Comunidad Autónoma de Madrid, Spain) is greatly acknowledged.

Supporting Information Available: X-ray diffractograms with 2θ angles ranging from 20° to 120° and Williamson-Hall (WH) plots for microstrain calculation are presented. This material is available free of charge via the Internet at http://pubs.acs.org

References

1. Xia, Z.; Xu, Z.; Chen, M.Liu, Q. Recent developments in the new inorganic solid-state LED phosphors. *Dalton Trans. 2016,* ***45****,(28)*, 11214-11232.
2. Xie, R.-J.; Li, Y. Q.; Hirosaki, N.Yamamoto, H., *Nitride Phosphors and Solid-State Lighting*. 2011, CRC Press
3. Lécuyer, C. Ueyama, T. The Logics of Materials Innovation The Case of Gallium Nitride and Blue Light Emitting Diodes. *HIST STUD NAT SCI 2013,* ***43****,(3)*, 243-280.
4. van Krevel, J. W. H.; Hintzen, H. T.; Metselaar, R.Meijerink, A. Long wavelength Ce^{3+} emission in Y–Si–O–N materials. *J. Alloys Compd. 1998,* ***268****,(1–2)*, 272-277.
5. Dierre, B.; Xie, R.-J.; Hirosaki, N.Sekiguchi, T. Blue emission of Ce^{3+} in lanthanide silicon oxynitride phosphors. *J. Mater. Res. 2007,* ***22****,(7)*, 1933-1941.
6. Li, Y. Q.; de With, G.Hintzen, H. T. Luminescence properties of Ce^{3+}-activated alkaline earth silicon nitride $M_2Si_5N_8$ (M=Ca, Sr, Ba) materials. *J. Lumin. 2006,* ***116****,(1–2)*, 107-116.
7. Wang, X.-M.; Wang, C.-H.; Kuang, X.-J.; Zou, R.-Q.; Wang, Y.-X.Jing, X.-P. Promising Oxonitridosilicate Phosphor Host $Sr_3Si_2O_4N_2$: Synthesis, Structure, and Luminescence Properties Activated by Eu^{2+} and Ce^{3+}/Li^{+} for pc-LEDs. *Inorg. Chem. 2012,* ***51****,(6)*, 3540-3547.
8. Inoue, K.; Hirosaki, N.; Xie, R.-J.Takeda, T. Highly Efficient and Thermally Stable Blue-Emitting AlN:Eu^{2+} Phosphor for Ultraviolet White Light-Emitting Diodes. *J. Phys. Chem. C 2009,* ***113****,(21)*, 9392-9397.
9. Sontakke, A. D.; Ueda, J.; Xu, J.; Asami, K.; Katayama, M.; Inada, Y.Tanabe, S. A Comparison on Ce^{3+} Luminescence in Borate Glass and YAG Ceramic: Understanding the Role of Host's Characteristics. *J. Phys. Chem. C 2016,* ***120****,(31)*, 17683-17691.
10. Martin, N. Scintillation detectors for x-rays. *Meas. Sci. Technol. 2006,* ***17****,(4)*, R37.
11. Zhao, Z.; Yang, Z.; Shi, Y.; Wang, C.; Liu, B.; Zhu, G.Wang, Y. Red-emitting oxonitridosilicate phosphors $Sr_2SiN_zO_{4-1.5z}$:Eu^{2+} for white light-emitting diodes: structure and luminescence properties. *J. Mater. Chem. C 2013,* ***1****,(7)*, 1407-1412.
12. Marchand, R.; Laurent, Y.; Guyader, J.; L'Haridon, P.Verdier, P. Nitrides and oxynitrides: Preparation, crystal chemistry and properties. *J. Eur. Ceram. Soc. 1991,* ***8****,(4)*, 197-213.
13. Rong-Jun, X. Naoto, H. Silicon-based oxynitride and nitride phosphors for white LEDs—A review. *Sci. Tech. Adv. Mater 2007,* ***8****,(7-8)*, 588.

14. He, X.-H.; Lian, N.; Sun, J.-H.Guan, M.-Y. Dependence of luminescence properties on composition of rare-earth activated (oxy)nitrides phosphors for white-LEDs applications. *J. Mater. Sci. 2009, **44**,(18)*, 4763-4775.
15. Guo, Q. Yoshida, A. Temperature Dependence of Band Gap Change in InN and AlN. *Jpn. J. Appl. Phys. 1994, **33**,(5R)*, 2453.
16. Aldabergenova, S. B.; Osvet, A.; Frank, G.; Strunk, H. P.; Taylor, P. C.Andreev, A. A. Blue, green and red emission from Ce^{3+}, Tb^{3+} and Eu^{3+} ions in amorphous GaN and AlN thin films. *J. Non-Cryst. Solids 2002, **299–302, Part 1***, 709-713.
17. Liu, T.-C.; Kominami, H.; Greer, H. F.; Zhou, W.; Nakanishi, Y.Liu, R.-S. Blue Emission by Interstitial Site Occupation of Ce^{3+} in AlN. *Chem. Mater. 2012, **24**,(17)*, 3486-3492.
18. Ishikawa, R.; Lupini, A. R.; Oba, F.; Findlay, S. D.; Shibata, N.; Taniguchi, T.; Watanabe, K.; Hayashi, H.; Sakai, T.; Tanaka, I.; Ikuhara, Y.Pennycook, S. J. Atomic Structure of Luminescent Centers in High-Efficiency Ce-doped w-AlN Single Crystal. *Sci. Rep. 2014, **4***, 3778.
19. Ishikawa, R.; Mishra, R.; Lupini, A. R.; Findlay, S. D.; Taniguchi, T.; Pantelides, S. T.Pennycook, S. J. Direct Observation of Dopant Atom Diffusion in a Bulk Semiconductor Crystal Enhanced by a Large Size Mismatch. *Phys. Rev. Lett. 2014, **113**,(15)*, 155501.
20. Dar, A. Majid, A. DFT study of cerium doped aluminum nitride. *Eur. Phys. J. Appl. Phys. 2015, **71**,(1)*, 10101.
21. Majid, A.; Asghar, F.; Rana, U. A.; Ud-Din Khan, S.; Yoshiya, M.; Hussain, F.Ahmad, I. Role of nitrogen vacancies in cerium doped aluminum nitride. *J. Magn. Magn. Mater. 2016, **412***, 49-54.
22. Wieg, A. T.; Penilla, E. H.; Hardin, C. L.; Kodera, Y.Garay, J. E. Broadband white light emission from Ce:AlN ceramics: High thermal conductivity down-converters for LED and laser-driven solid state lighting. *APL Materials 2016, **4**,(12)*, 126105.
23. Yokoyama, T.; Iwazaki, Y.; Onda, Y.; Nishihara, T.; Sasajima, Y.Ueda, M. Effect of Mg and Zr co-doping on piezoelectric AlN thin films for bulk acoustic wave resonators. *IEEE Trans. Ultrason., Ferroelect., Freq. Control 2014, **61**,(8)*, 1322-1328.
24. Nilsson, D.; Janzén, E.Kakanakova-Georgieva, A. Lattice parameters of AlN bulk, homoepitaxial and heteroepitaxial material. *J. Phys. D: Appl. Phys. 2016, **49**,(17)*, 175108.
25. Liu, F. S.; Liu, Q. L.; Liang, J. K.; Luo, J.; Zhang, H. R.; Zhang, Y.; Sun, B. J.Rao, G. H. Visible and infrared emissions from c-axis oriented AlN:Er films grown by magnetron sputtering. *J. Appl. Phys. 2006, **99**,(5)*, 053515.
26. Liu, B.; Gao, J.; Wu, K. M.Liu, C. Preparation and rapid thermal annealing of AlN thin films grown by molecular beam epitaxy. *Solid State Commun. 2009, **149**,(17–18)*, 715-717.
27. Mao, C.; Li, W.; Wu, F.; Dou, Y.; Fang, L.; Ruan, H.Kong, C. Effect of Er doping on microstructure and optical properties of ZnO thin films prepared by sol–gel method. *J. Mater. Sci. - Mater. Electron. 2015, **26**,(11)*, 8732-8739.
28. Stan, G. E.; Pasuk, I.; Galca, A. C.Dinescu, A. Highly textured (001) AlN nanostructured thin films synthesized by reactive magnetron sputtering for SAW and FBAR applications. *Dig J Nanomater Biostruct 2010, **5**,(4)*.
29. Balzar, D. X-Ray Diffraction Line Broadening: Modeling and Applications to High-T(c) Superconductors. *J Res Natl Inst Stand Technol 1993, **98**,(3)*, 321-353.
30. Lorenz, K.; Nogales, E.; Nédélec, R.; Penner, J.; Vianden, R.; Alves, E.; Martin, R. W.O`Donnell, K. P. Influence of the Annealing Ambient on Structural and Optical Properties of Rare Earth Implanted GaN. *MRS Proceedings 2005, **892***.

31. Lin, C.-Y. Lu, F.-H. Oxidation behavior of AlN films at high temperature under controlled atmosphere. *J. Eur. Ceram. Soc. 2008,* ***28****,(3)*, 691-698.
32. Slack, G. A. Nonmetallic crystals with high thermal conductivity. *J. Phys. Chem. Solids 1973,* ***34****,(2)*, 321-335.
33. Rosa, J. Tale, I. Mechanism of thermoluminescence in AlN:O. *Czech J Phys B 1979,* ***29****,(7)*, 810-824.
34. Slack, G. A.; Schowalter, L. J.; Morelli, D.Freitas Jr, J. A. Some effects of oxygen impurities on AlN and GaN. *J. Cryst. Growth 2002,* ***246****,(3–4)*, 287-298.
35. Berzina, B.; Trinkler, L.; Sils, J.Atobe, K. Luminescence mechanisms of oxygen-related defects in AlN. *Radiat Eff. Defects Solids 2002,* ***157****,(6-12)*, 1089-1092.
36. Yan, Q.; Janotti, A.; Scheffler, M.Van de Walle, C. G. Origins of optical absorption and emission lines in AlN. *Appl. Phys. Lett. 2014,* ***105****,(11)*, 111104.
37. Sedhain, A.; Du, L.; Edgar, J. H.; Lin, J. Y.Jiang, H. X. The origin of 2.78 eV emission and yellow coloration in bulk AlN substrates. *Appl. Phys. Lett. 2009,* ***95****,(26)*, 262104.
38. Vila, M.; Díaz-Guerra, C.; Jerez, D.; Lorenz, K.; Piqueras, J.Alves, E. Intense luminescence emission from rare-earth-doped MoO_3 nanoplates and lamellar crystals for optoelectronic applications. *J. Phys. D: Appl. Phys. 2014,* ***47****,(35)*, 355105.
39. Sakaguchi, I.; Ohgaki, T.; Adachi, Y.; Hishita, S.; Ohashi, N.Haneda, H. Effect of post-annealing on structural and optical properties, and elemental distribution in heavy Eu-implanted ZnO thin films. *J. Ceram. Soc. Jpn. 2010,* ***118****,(1383)*, 1087-1089.
40. Zanatta, A. R. Effect of thermal annealing treatments on the optical properties of rare-earth-doped AlN films. *J. Phys. D: Appl. Phys. 2009,* ***42****,(2)*, 025109.
41. Chin, W. C. Cheong, K. Y. Effects of post-deposition annealing temperature and ambient on RF magnetron sputtered Sm_2O_3 gate on n-type silicon substrate. *J. Mater. Sci. - Mater. Electron. 2011,* ***22****,(12)*, 1816.
42. Rao, T. P.; Raj, S. G.Kumar, M. C. S. Effect of Annealing Atmosphere on Structural and Optical Properties of Nd:ZnO Thin Films. *Procedia Mater. Sci. 2014,* ***6***, 1631-1638.
43. Zhang, Q. Y.; Pita, K.; Ye, W.Que, W. X. Influence of annealing atmosphere and temperature on photoluminescence of Tb^{3+} or Eu^{3+}-activated zinc silicate thin film phosphors via sol–gel method. *Chem. Phys. Lett. 2002,* ***351****,(3–4)*, 163-170.
44. Wu, L.; Wiesmann, H. J.; Moodenbaugh, A. R.; Klie, R. F.; Zhu, Y.; Welch, D. O.Suenaga, M. Oxidation state and lattice expansion of CeO_{2-x} nanoparticles as a function of particle size. *Phys.Rev.B 2004,* ***69****,(12)*, 125415.
45. Cheng, S.; Yang, G.; Zhao, Y.; Peng, M.; Skibsted, J.Yue, Y. Quantification of the boron speciation in alkali borosilicate glasses by electron energy loss spectroscopy. *Sci. Rep. 2015,* ***5***, 17526.
46. Stampfl, C. Van de Walle, C. G. Theoretical investigation of native defects, impurities, and complexes in aluminum nitride. *Phys.Rev.B 2002,* ***65****,(15)*, 155212.
47. Mäki, J. M.; Makkonen, I.; Tuomisto, F.; Karjalainen, A.; Suihkonen, S.; Räisänen, J.; Chemekova, T. Y.Makarov, Y. N. Identification of the V_{Al}-O_N defect complex in AlN single crystals. *Phys.Rev.B 2011,* ***84****,(8)*, 081204.
48. Sedhain, A.; Nepal, N.; Nakarmi, M. L.; Al tahtamouni, T. M.; Lin, J. Y.; Jiang, H. X.; Gu, Z.Edgar, J. H. Photoluminescence properties of AlN homoepilayers with different orientations. *Appl. Phys. Lett. 2008,* ***93****,(4)*, 041905.
49. Nepal, N.; Nakarmi, M. L.; Lin, J. Y.Jiang, H. X. Photoluminescence studies of impurity transitions in AlGaN alloys. *Appl. Phys. Lett. 2006,* ***89****,(9)*, 092107.
50. Nam, K. B.; Nakarmi, M. L.; Lin, J. Y.Jiang, H. X. Deep impurity transitions involving cation vacancies and complexes in AlGaN alloys. *Appl. Phys. Lett. 2005,* ***86****,(22)*, 222108.

51. Hoshi, T.; Koyama, T.; Sugawara, M.; Uedono, A.; Kaeding, J. F.; Sharma, R.; Nakamura, S.Chichibu, S. F. Correlation between the violet luminescence intensity and defect density in AlN epilayers grown by ammonia-source molecular beam epitaxy. *Phys. Status Solidi C 2008, **5**,(6)*, 2129-2132.
52. Lu, P.; Collazo, R.; Dalmau, R. F.; Durkaya, G.; Dietz, N.Sitar, Z. Different optical absorption edges in AlN bulk crystals grown in m- and c-orientations. *Appl. Phys. Lett. 2008, **93**,(13)*, 131922.
53. Paul, A.; Mulholland, M.Zaman, M. S. Ultraviolet absorption of cerium(III) and cerium(IV) in some simple glasses. *J. Mater. Sci. 1976, **11**,(11)*, 2082-2086.
54. Herrmann, A.; Othman, H. A.; Assadi, A. A.; Tiegel, M.; Kuhn, S.Rüssel, C. Spectroscopic properties of cerium-doped aluminosilicate glasses. *Opt. Mater. Express 2015, **5**,(4)*, 720-732.
55. Brandily-Anne, M.-L.; Lumeau, J.; Glebova, L.Glebov, L. B. Specific absorption spectra of cerium in multicomponent silicate glasses. *J. Non-Cryst. Solids 2010, **356**,(44–49)*, 2337-2343.
56. He, X.; Liu, X.; Li, R.; Yang, B.; Yu, K.; Zeng, M.Yu, R. Effects of local structure of Ce^{3+} ions on luminescent properties of $Y_3Al_5O_{12}$:Ce nanoparticles. *Sci. Rep. 2016, **6***, 22238.
57. O'Donnell;, K. Dierolf, V. eds. Rare-Earth Doped III-Nitrides for Optoelectronic and Spintronic Applications; *Springer Netherlands:2010; Vol. 124.*
58. Kenyon, A. J. Recent developments in rare-earth doped materials for optoelectronics. *Prog. Quantum Electron. 2002, **26**,(4–5)*, 225-284.

Figure captions

Figure 1: XRD of as-deposited and annealed undoped and Ce-doped AlN films.

Figure 2: TEM images and corresponding SAED patterns for undoped AlN (a, b), CeAlN_As (c, d), CeAlN_FG (e, f) and CeAlN_Ar (g, h). Inset of fig (2 g): Magnification on a part of top layer of CeAlN_Ar sample.

Figure 3: RBS fitting data for the CeAlN as-deposited and annealed in Ar films. Inset: table with the atomic content of film constitutive elements for the best fitting of RBS data.

Figure 4: PL of undoped and Ce-doped AlN films excited by a) 325 nm and b) 266 lasers. Inset of fig (4 a): Magnification on the very weak spectra for clarification. Inset photo image: visible blue light emitted from the photo-excited CeAlN_Ar film.

Figure 5: EELS at Ce M-edges peaks for a) CeO_2 and CeF_3 reference samples, b) CeAlN_As, CeAlN_FG and CeAlN_Ar. Arrows are to guide the reader to the peak shoulders in the spectra.

Figure 6: PLE spectra recorded at emission peak 500 nm for the CeAlN_Ar film.

Figure 7: PL of two CeAlN samples annealed in Ar and prepared at Al-rich and N-rich conditions.

Figures

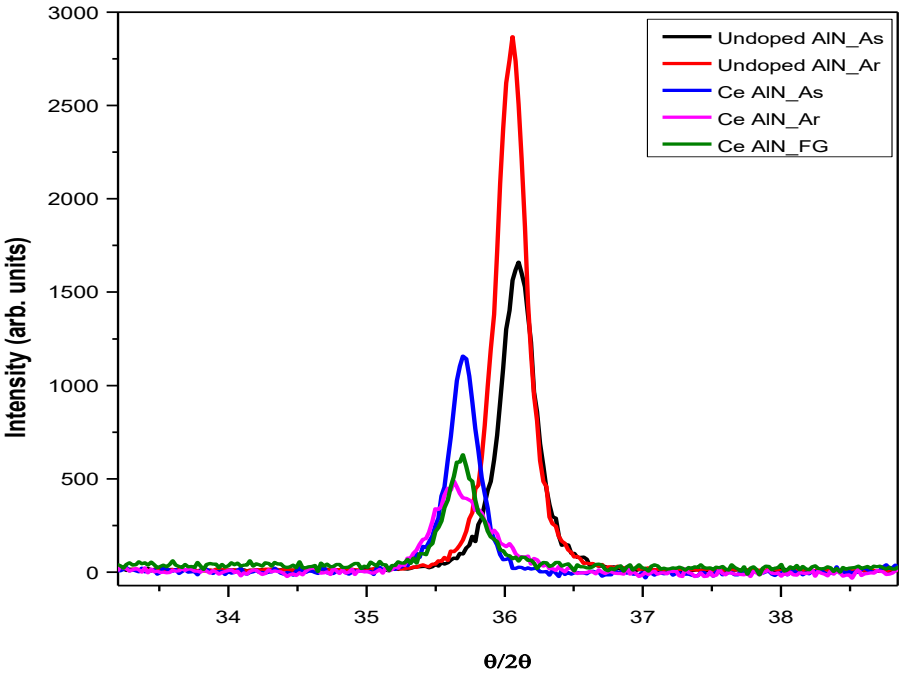

Figure 1: XRD of as-deposited and annealed undoped and Ce-doped AlN films.

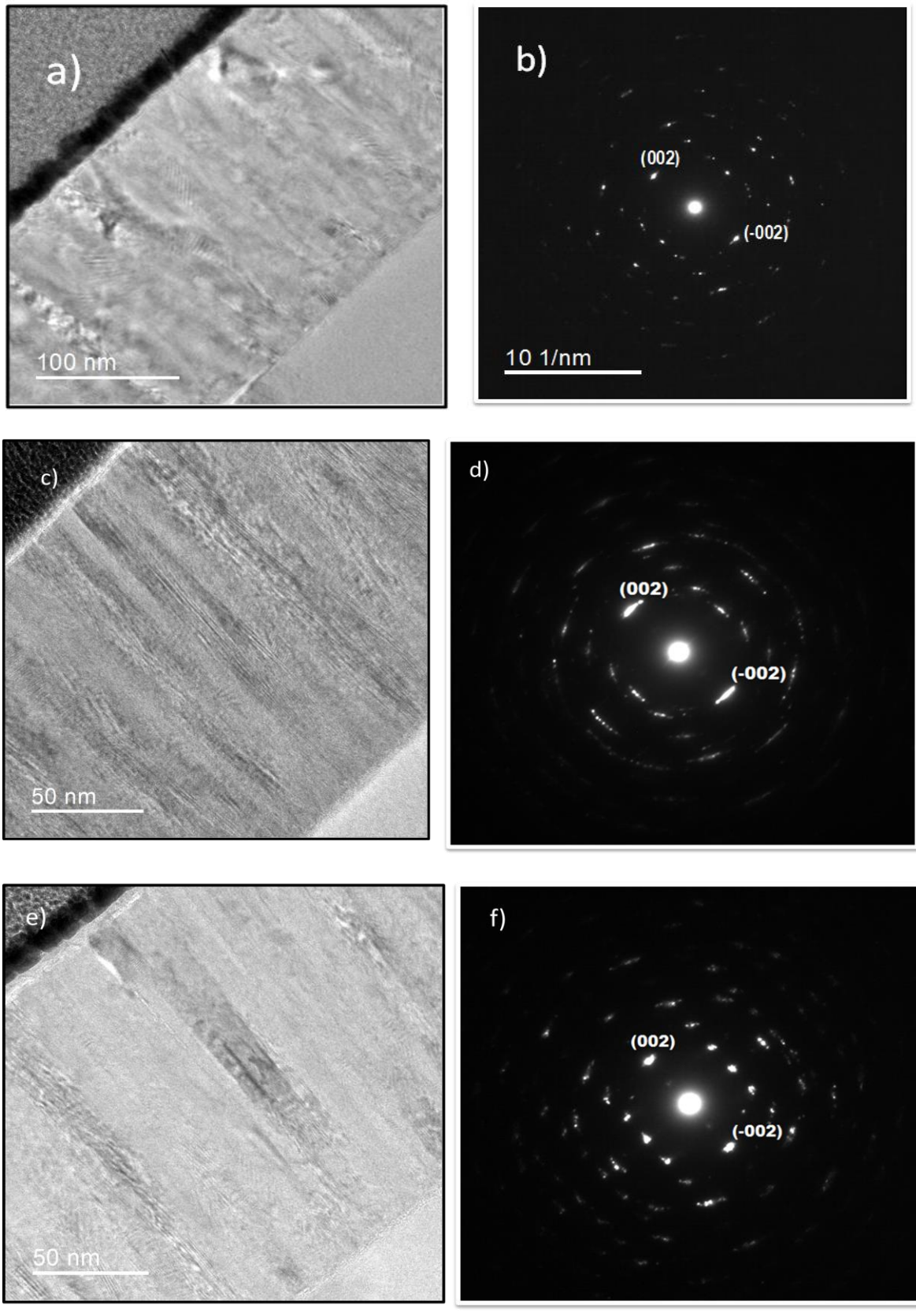
a)
100 nm
b)
(002)
(-002)
10 1/nm
c)
50 nm
d)
(002)
(-002)
e)
50 nm
f)
(002)
(-002)

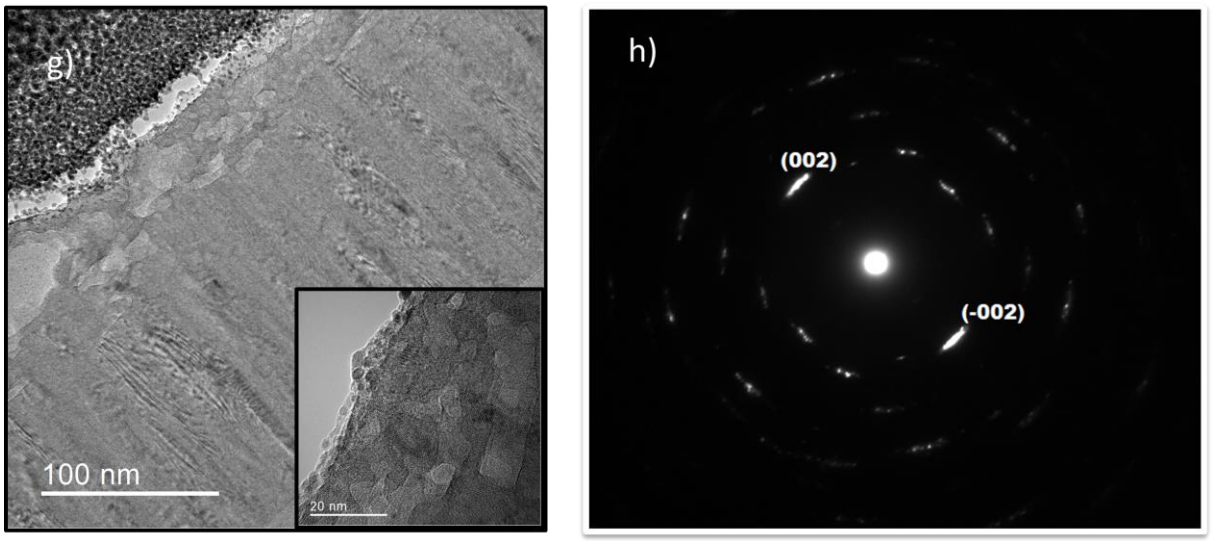

Figure 2: TEM images and corresponding SAED patterns for undoped AlN (a, b), CeAlN_As (c, d), CeAlN_FG (e, f) and CeAlN_Ar (g, h). Inset of fig (2 g): Magnification on a part of top layer of CeAlN_Ar sample.

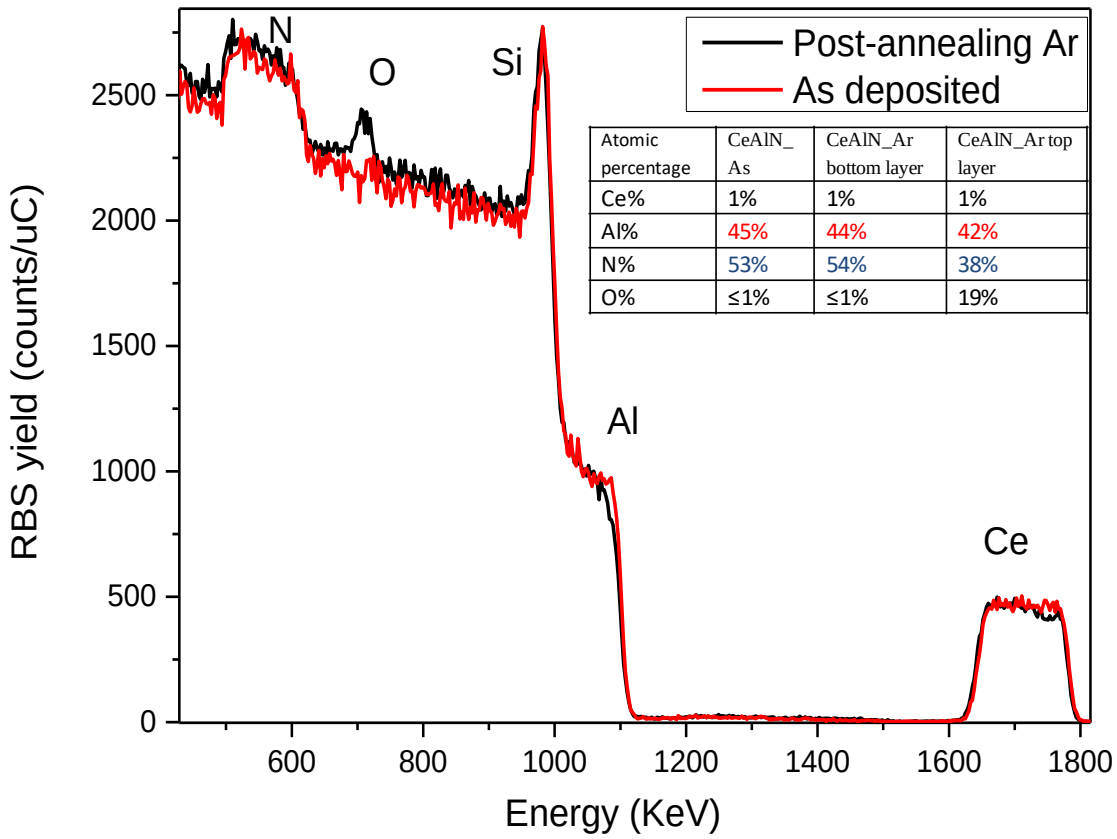

Atomic percentage	CeAlN_ As	CeAlN_Ar bottom layer	CeAlN_Ar top layer
Ce%	1%	1%	1%
Al%	45%	44%	42%
N%	53%	54%	38%
O%	≤1%	≤1%	19%

Figure (3): RBS fitting data for the CeAlN as-deposited and annealed in Ar films. Inset: table with the atomic content of film constitutive elements for the best fitting of RBS data.

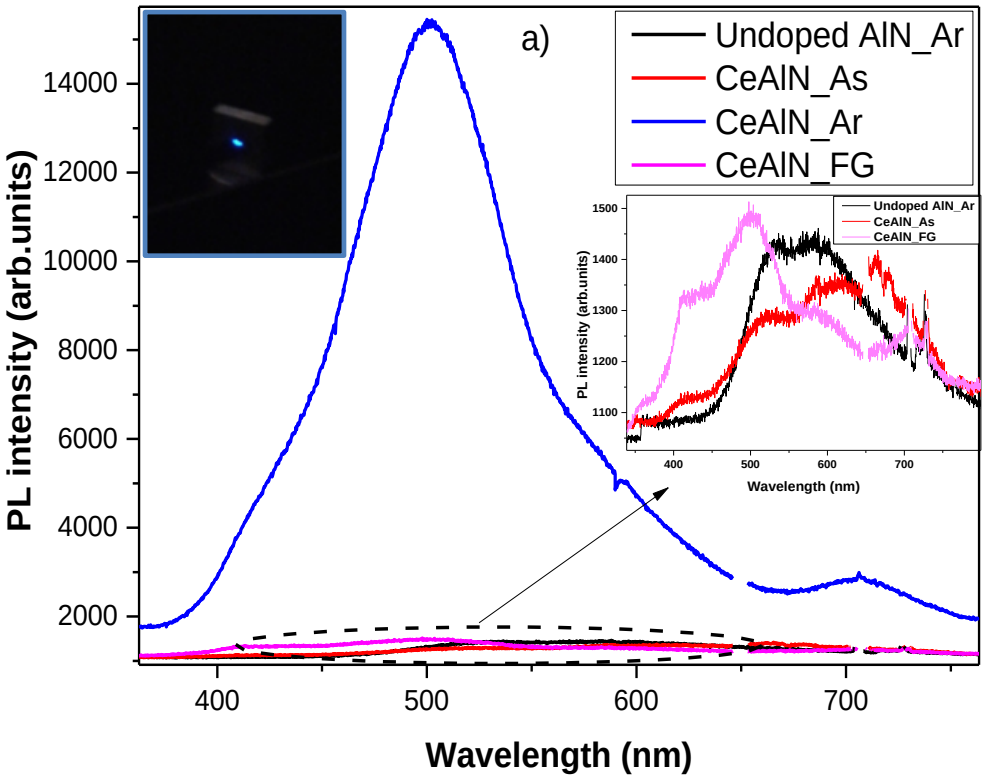
a)
Undoped AlN_Ar
CeAlN_As
CeAlN_Ar
CeAlN_FG
PL intensity (arb.units)
Wavelength (nm)
14000
12000
10000
8000
6000
4000
2000
400
500
600
700
1500
1400
1300
1200
1100

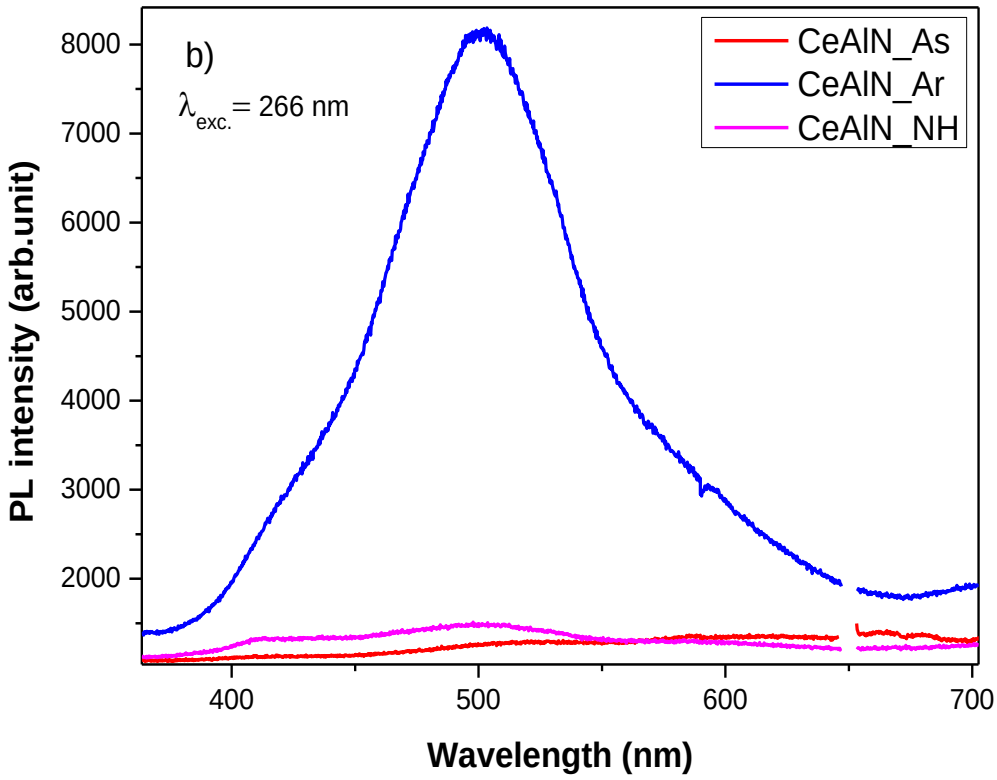

Figure 4: PL of undoped and Ce-doped AlN films excited by a) 325 nm and b) 266 lasers. Inset of fig (4 a): Magnification on the very weak spectra for clarification. Inset photo image: visible blue light emitted from the photo-excited CeAlN_Ar film.

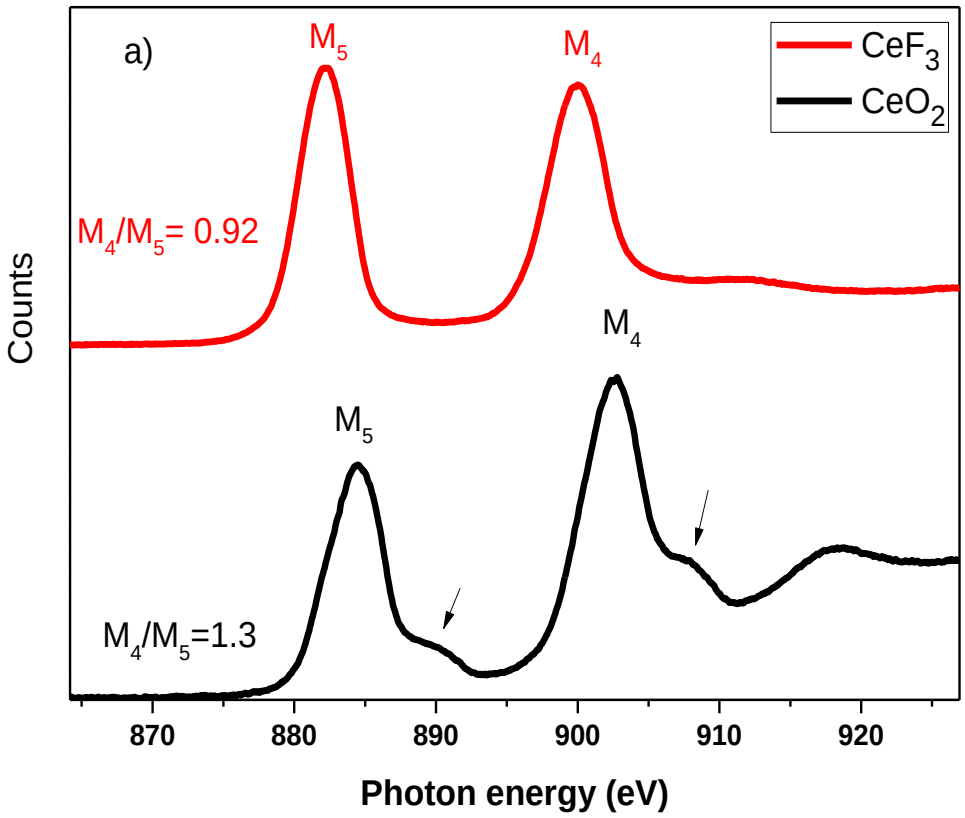
a)
M5
M4
CeF3
CeO2
M4/M5= 0.92
Counts
M4
M5
M4/M5=1.3
870
880
890
900
910
920
Photon energy (eV)

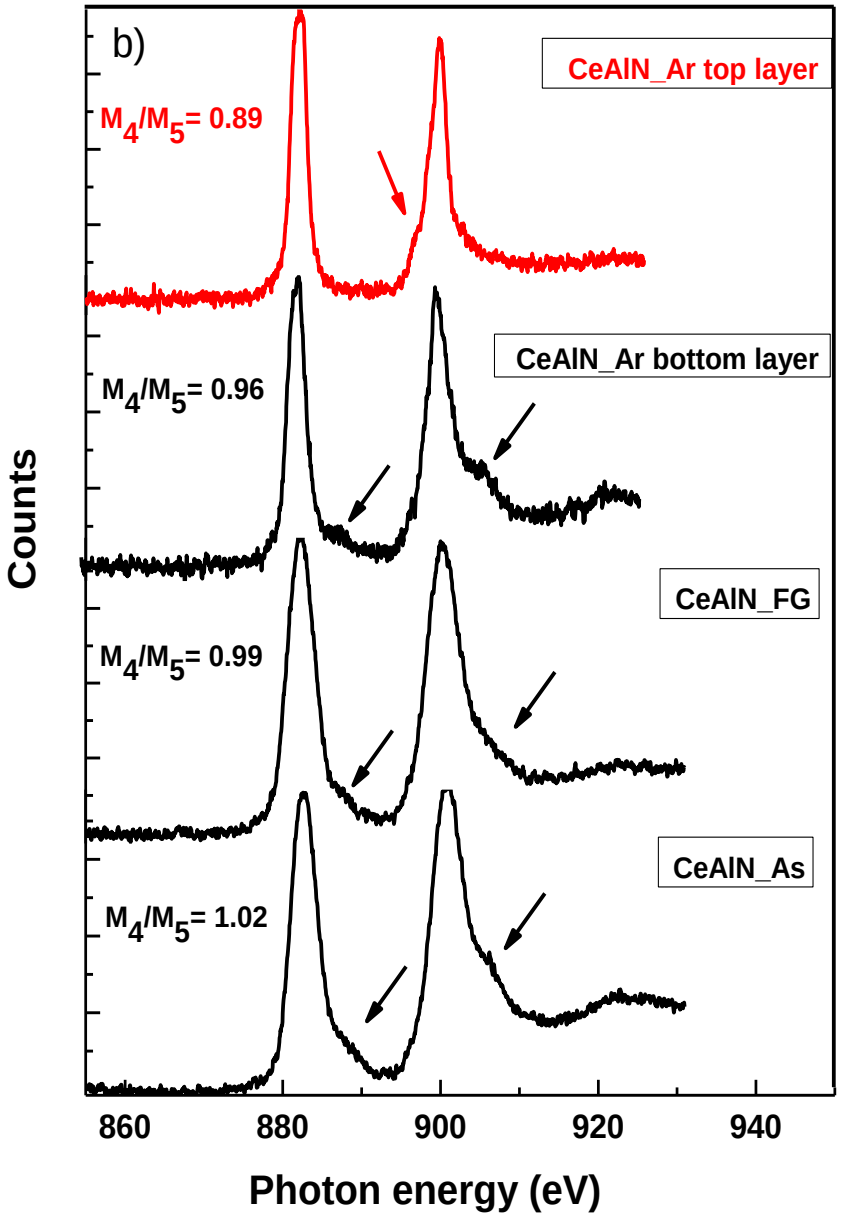

Figure 5: EELS at Ce M-edges peaks for a) CeO_2 and CeF_3 reference samples, b) CeAlN_As, CeAlN_FG and CeAlN_Ar. Arrows are to guide the reader to the peak shoulders in the spectra.

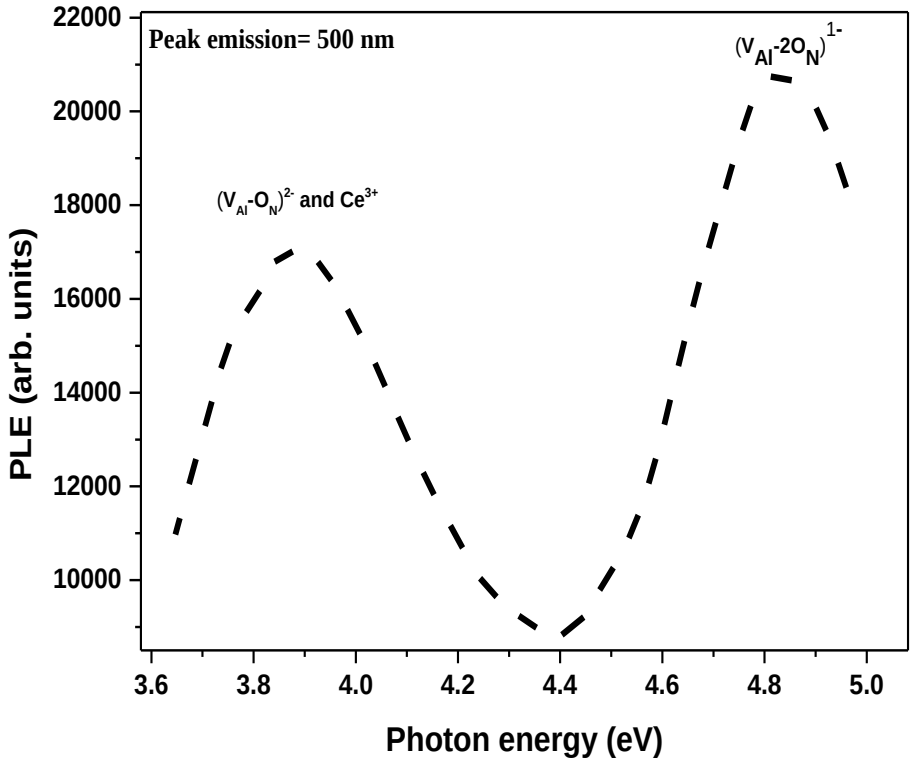

Figure 6: PLE spectra recorded at emission peak 500 nm for the CeAlN_Ar film.

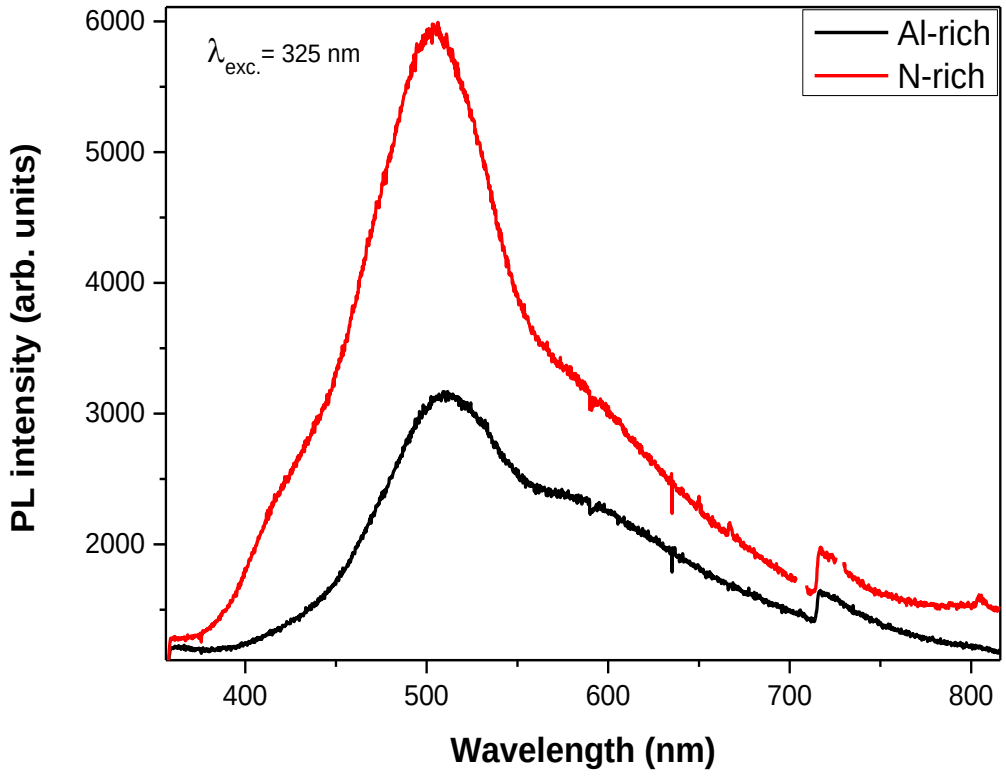

Figure 7: PL of two CeAlN samples annealed in Ar and prepared at Al-rich and N-rich conditions.